IN-75-CR
51897
P 26

A SIMULATION STUDY OF INTERACTIONS OF SPACE-SHUTTLE GENERATED ELECTRON BEAMS WITH AMBIENT PLASMA AND NEUTRAL GAS

NASA Headquarters

Contract No. NAGW-1936

SwRI Project No. 15-3399

Annual Progress Report

Robert M. Winglee
Project Manager

(NASA-CR-189019) A SIMULATION STUDY OF INTERACTIONS OF SPACE-SHUTTLE GENERATED ELECTRON BEAMS WITH AMBIENT PLASMA AND NEUTRAL GAS Annual Progress Report (Southwest Research Inst.) 26 p CSCL 20I G3/75

N92-14846

Unclas
0051897

Introduction

This report summarizes results obtained during the period from November 1990 to November 1991. The objective of this project is to conduct large scale simulations of electron beams injected into space. We have completed two papers and presented them at 1991 Cambridge Workshop in Theoretical Geoplasma Physics during June 24-28, 1991. The first paper entitled "Simulations of the active injection of electron beams" by Dr. R. M. Winglee is included in this report as Appendix A, and the second paper entitled "Simulations of radial expansion of an injected electron beam" by J. Koga and C. S. Lin is included here as Appendix B. The results are briefly summarized below.

Summary of Progress

Simulations of the Active Injections of Electron Beams

The study of the active injection of electron beams from spacecraft is important as it provides valuable insight into beam-plasma interactions and the development of current systems in the ionosphere. However, the beam injection itself is not simple, being constrained by the ability of the spacecraft to draw return current from the ambient plasma. The generation of these return currents is dependent on several factors including the density of the ambient plasma relative to the beam density, the presence of neutrals around the spacecraft, the configuration of the spacecraft and the motion of the spacecraft through the plasma. Two dimensional (three velocity) particle simulations with collisional processes included are used to show how these different and often coupled processes can be utilized to enhance beam propagation from the spacecraft.

Simulation of Radial Expansion of an Injected Electron Beam

To understand the radial expansion mechanism of an electron beam injected from a highly charged spacecraft, two-dimensional particle-in-cell simulations are conducted for a high density electron beam injected parallel to magnetic fields from an isolated equipotential conductor into a cold background plasma. The simulations indicate that charge buildup at the beam stagnation point causes the beam to expand radially to the beam electron gyroradius.

Future Plan

We have just received the second year funding and we will resume working on the project. In the next year we will prepare an article reporting a parameter survey of the beam radius after injecting from a conductor. From the simulation results, we will determine the dependence of beam radius on magnetic field, beam density, beam energy, and other plasma parameters. In addition, we will apply the beam injection simulation techniques developed for studying electron beam injections from the Shuttle to study the magnetosheath plasma injections into the polar cusp. A cusp magnetic field topology will be used in a two dimension simulations. The simulation boundary will include a large cold plasma at one boundary to represent the ionosphere and an injected hot plasma at another boundary representing the magnetosheath. We expect that the injected ions and electrons will follow different field lines,

causing charge separation. The simulation work would be important for modeling the ionospheric feedback effects in the Earth's polar cusp region.

APPENDIX A

SIMULATIONS OF THE ACTIVE INJECTION OF ELECTRON BEAMS

R. M. WINGLEE
Department of Space Sciences, Southwest Research Institute
PO. Drawer 28510, San Antonio, TX 78228-0510

ABSTRACT

The study of the active injection of electron beams from spacecraft is important as it provides valuable insight into beam-plasma interactions and the development of current systems in the ionosphere. However, the beam injection itself is not simple, being constrained by the ability of the spacecraft to draw return current from the ambient plasma. The generation of these return currents is dependent on several factors including the density of the ambient plasma relative to the beam density, the presence of neutrals around the spacecraft, the configuration of the spacecraft and the motion of the spacecraft through the plasma. Two dimensional (three velocity) particle simulations with collisional processes included are used to show how these different and often coupled processes can be utilized to enhance beam propagation from the spacecraft.

I. INTRODUCTION

Over the past ten years there have been several space experiments which utilize electron beams injected from spacecraft to study beam-plasma interactions and the development of current systems in space plasmas. Recent or continuing active experiments which employ electron beams include: (i) the ECHO program [1–6], (ii) the Space Experiments with Particle Accelerators, SEPAC, and the Vehicle Charging And Potential, VCAP, experiments on the Space Shuttle [7–13], (iii) MAIMIK [14–15] and (iv) the Cooperative High Altitude Rocket Gun Experiments, CHARGE [16-18].

While understanding the characteristics of the beam-plasma interaction and the induced currents is central to the above experiments, there are fundamentally important differences in the beam and spacecraft configuration which can significantly alter the characteristics of the interaction between the different experiments. For example, in the early experiments the beam was injected from a single spacecraft where most of the diagnostics were confined. As it became more evident that significant spacecraft charging could be occurring and that effects from the beam-plasma interaction were not restricted to just the beam region, the emphasis in the more recent experiments has been to investigate the induced plasma phenomena via diagnostic packages ejected from the beam-emitting (mother) payload.

If in addition, these ejected payloads remained electrically connected via a tether wire, spacecraft charging could conceivably be reduced by the collection of current by the ejected payload at extended distances across the field lines. Such a tethered (daughter) payload was successfully deployed during CHARGE 2. Tethered payloads were also successfully deployed during Echo 7 and MAIMIK but in these experiments the tether impedance was made very high in order to measure the potential across the field lines rather than to collect current.

The results of CHARGE 2 are particularly interesting because they showed that in the absence of neutrals the percentage of current collected by the daughter payload tended to be smaller than its relative area, i.e. that the tethered payload is relatively inefficient in collecting current [18]. However, during thruster firings from the daughter payload, the daughter could collect a large fraction of the beam current. This current collection could be suppressed during thruster firings from the mother payload, irrespective of whether neutrals were being injected from the daughter.

Understanding the above results is not only important in itself but could possibly have important applications for the upcoming Shuttle Electrodynamics Tether Satellite (SETS). In this experiment, a satellite will be released from the shuttle along a tether that can extend up to 10 km. Power can be generated via the motion of the tether wire through the geomagnetic field if the tether current can be closed in the ionosphere via beam injection. While the geometry of SETS is very similar to that of CHARGE 2, one important difference is that in the sounding rocket experiments, the payloads are subsonic, moving at about 1 km/s, while the shuttle travelling at about 8 km/s is supersonic. As a result of this supersonic propagation, the current collecting characteristics of the spacecraft can be modified.

The purpose of this paper is to investigate the processes governing the return currents into the spacecraft for the different configurations to identify that configuration which best enables the beam to propagate away from the spacecraft with minimal distortion. The study utilizes two-dimensional (three velocity) electromagnetic particle simulations to self-consistently evaluate the current and beam characteristics as well as the heating of the ambinet plasma as functions of (a) the spacecraft configuration, (b) the injection of neutrals and (c) the motion of the spacecraft through the ambient plasma.

II. SIMULATION MODEL

The algorithm for the particle simulations is described in [20, 21]. These simulations allow the self-consistent evaluation of the beam-plasma interaction as well as effects from spacecraft charging and the ionization of neutrals. Schematics for the different spacecraft configurations considered are shown in Figure 1. The mother and daughter payloads are indicated by

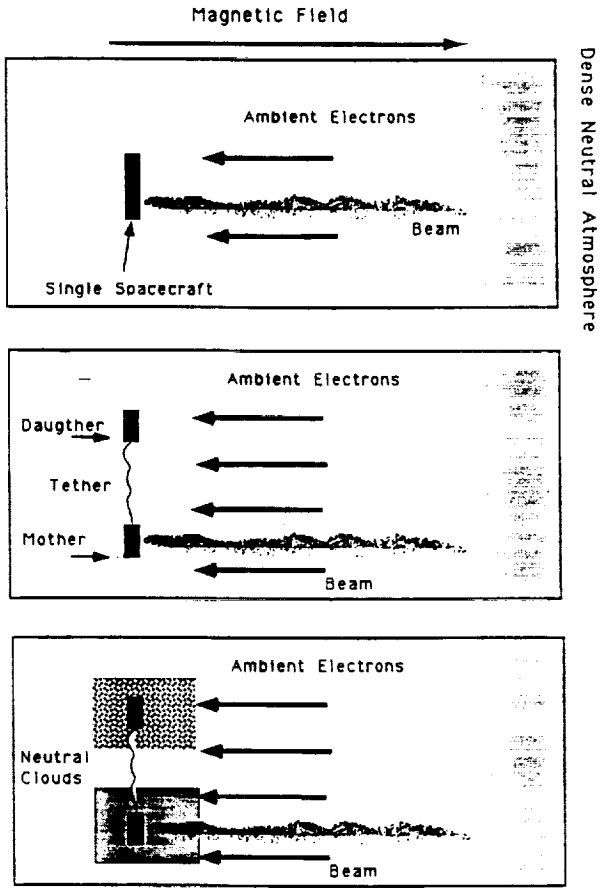

Fig. 1. Schematic showing the different spacecraft configurations. considered

the black rectangles and are of equal size with dimensions $4\Delta \times 16\Delta$ where the system size is $512\Delta \times 128\Delta$ and Δ is a plasma Debye length which is of the order of 10 cm for the parameters considered here. For the single spacecraft configuration, the two payloads are placed side-by-side (Fig. 1a) with both payloads kept at the same potential. The beam is injected from the middle of the lower (mother) payload at an angle of 45° to the magnetic field which is in the x-direction. The parallel velocity of the beam is assumed to be 10 times the ambient thermal velocity (i.e., $v_{xb} = 10v_{Te}$). Because of the limited resolution of the simulations the beam density is assumed to be smeared out over a slightly larger region than the actual beams used in the experiments and the beam density is correspondingly reduced so that the total beam current is comparable to that used in the CHARGE 2 experiment, i.e., about 100 mA. In the following, the beam width is taken to be 2Δ and the beam density density is assumed to be 4 times the ambient density which is of the order of 10^5 cm^{-3}, similar to [22]. The corresponding ambient plasma frequency ω_{pe} is equal to the

electron cyclotron frequency Ω_e and the (initial) beam plasma frequency ω_{pb} is equal to $2\omega_{pe}$.

For the tethered configurations, the mother and daughter payloads are separated by 64Δ across the field lines. With this separation, return currents can be generated over a larger distance across the field lines (Fig. 1b). Charge is moved between the two payloads so that both spacecraft are maintained at the same potential, essentially modelling the role of the tether wire. In addition, a voltage can be applied between the two payloads to shift in the potential of the payloads relative to the plasma potential and thereby modify their current collection capabilities.

As discussed in the following sections, the local plasma can become depleted due to return currents into the spacecraft, leading to the strong charging of the spacecraft, irrespective of the above spacecraft configurations. However, this plasma depletion can be overcome by the injection of neutrals and their ionization by energetic electrons (Fig. 1c). For simplicity, the neutral cloud is assumed to extend 50Δ behind the spacecraft and 100Δ in front with a width of 32Δ and a density of about 10^{11} cm^{-3}. This neutral cloud can be placed around either the mother or daughter.

III. BEAM INJECTION IN THE ABSENCE OF NEUTRALS

The evolution of the beam phase space for the single spacecraft and tether configurations are shown in Fig. 2. For the single spacecraft configuration, a stagnation region where some of the beam electrons are decelerated and eventually drawn back into the spacecraft (i.e., beam electrons with $v_x < 0$) quickly forms but, with neutralization by the return currents from the ambient plasma, some of the beam particles are able to escape and there is strong heating of the beam particles due to induced turbulence (Fig. 2a). At later times, the ambient plasma becomes depleted leading the reformation of the stagnation region (Fig. 2b). This stagnation region then remains a permanent feature until the beam is turned off (Fig. 2c) [20].

For the tether configuration, the beam is more easily able to propagate away from the spacecraft at early times (e.g., Figs. 2d and e). This enhanced propagation is due to the increased area over which return currents are drawn from the plasma when the payloads are separated across the field lines. Nevertheless, the local ambient plasma eventually becomes depleted as before and a stagnation region eventually forms (Fig. 2f). This depletion also occurs even if the daughter is biased positively and the mother negatively (phase spaces not shown). Thus, while the tether configuration allows enhanced current collection initially, the local depletion of plasma still leads to strong spacecraft charging and beam distortion.

The ability of the different payloads to collect current is illustrated in Fig. 3 which shows the time history of the relative current collected by

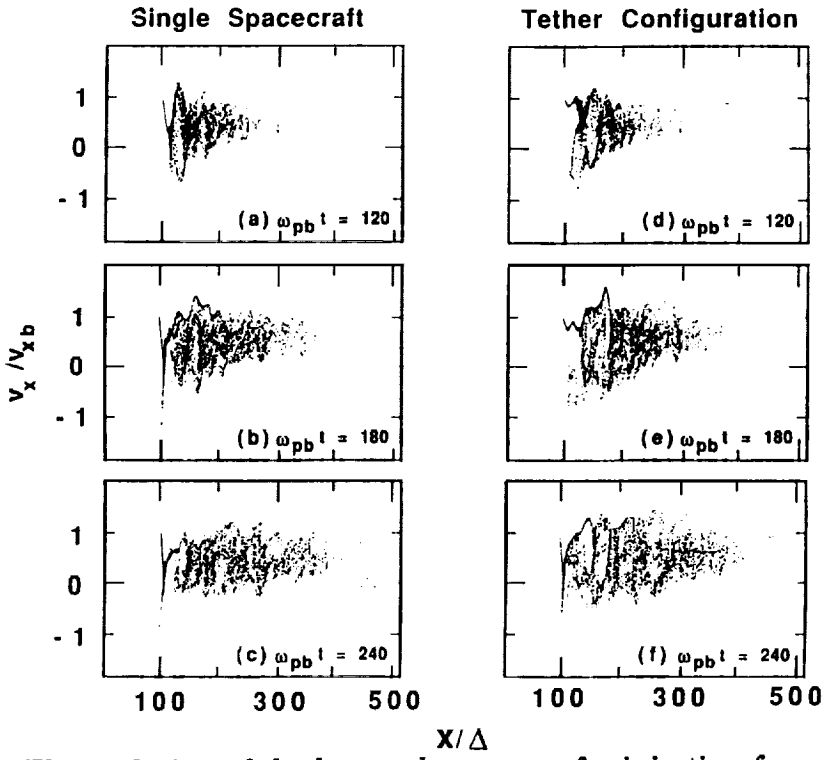

Fig. 2. The evolution of the beam phase space for injection from a single spacecraft (left hand side) and from a tethered configuration (right hand side).

the two payloads. In all cases, the beam is turned off at $\omega_{pb}t = 240$. For the single spacecraft configuration (Fig. 3a), it is seen that the daughter initially collects about 30% of the beam current even though it has the same surface area as the mother. The relative fraction collected by the daughter increases to a maximum of about 50% of the beam current at $\omega_{pb}t \simeq 120$, after which the depletion of the ambient plasma leads to a drop off in current collected. At this point the current collected by the mother increases. Much of this return current is, however, made up of reflected beam particles (as seen from the phase spaces in Fig. 2). After beam turnoff there is a rapid drop out in this component. However, the spacecraft continues net negative charge for about $60/\omega_{pb}$ after turnoff which causes the spacecraft to reach high negative potentials after beam turnoff.

For the tethered configuration (Fig. 3b), the amount of return current collected by the daughter increases until about $180/\omega_{pb}$, which is about a 50% increase on the period seen in the single spacecraft configuration. The current collected by the daughter can be further enhanced by making the daughter positively biased and the mother negatively biased. This enhancement is illustrated in Fig. 3c. In this case, the daughter is able to collect nearly 0.8 of the beam current during the first half of the beam

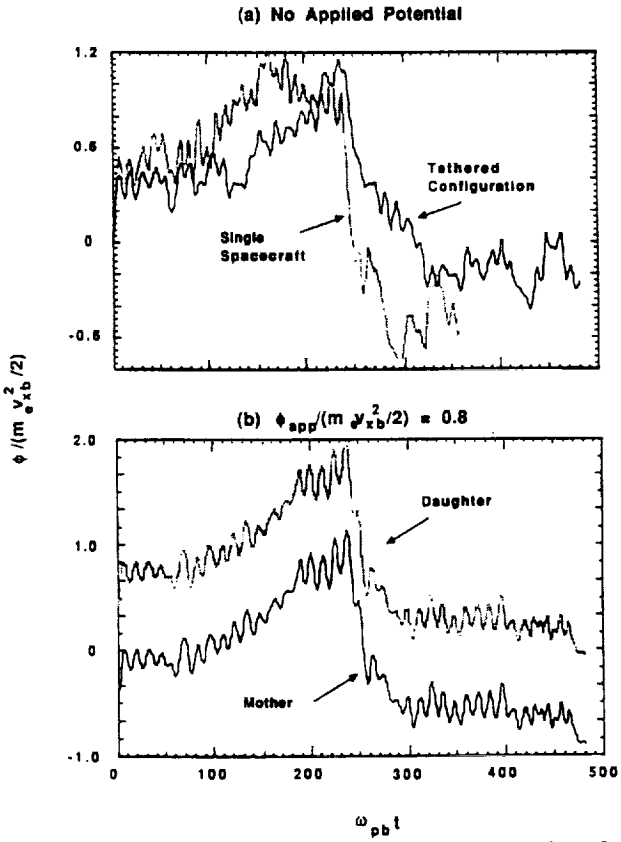

Fig. 3. Time histories of the current collected by the daughter (dotted lines) and the mother (solid lines) for (a) the single spacecraft configuration, (b) the tether configuration and (c) when a voltage equal to 80% of the parallel beam energy is applied between mother and daughter. The beam is turned off at $\omega_{pb}t = 240$.

injection. However, in both cases the depletion of the local plasma leads to a drop out in the daughters ability to collect current.

Fig. 4 shows the time histories of the potentials of the mother and daughter corresponding to Fig. 3. In all cases, when the local plasma becomes deleted, the potential of the beam-emitting payload increases to about the parallel energy of the beam. This is true even if a potential is applied between the payloads to make the initial potential of the beam-emitting payload negative.

IV. BEAM INJECTION IN THE PRESENCE OF NEUTRALS

The above results show that the depletion of the ambient plasma can lead to strong spacecraft charging. This effect can be offset with the injection of neutral (e.g., during thruster firings) and the subsequent ionization by energetic electrons can lead to the replenishment of the ambient plasma. This effect is well documented experimentally [18] and has been

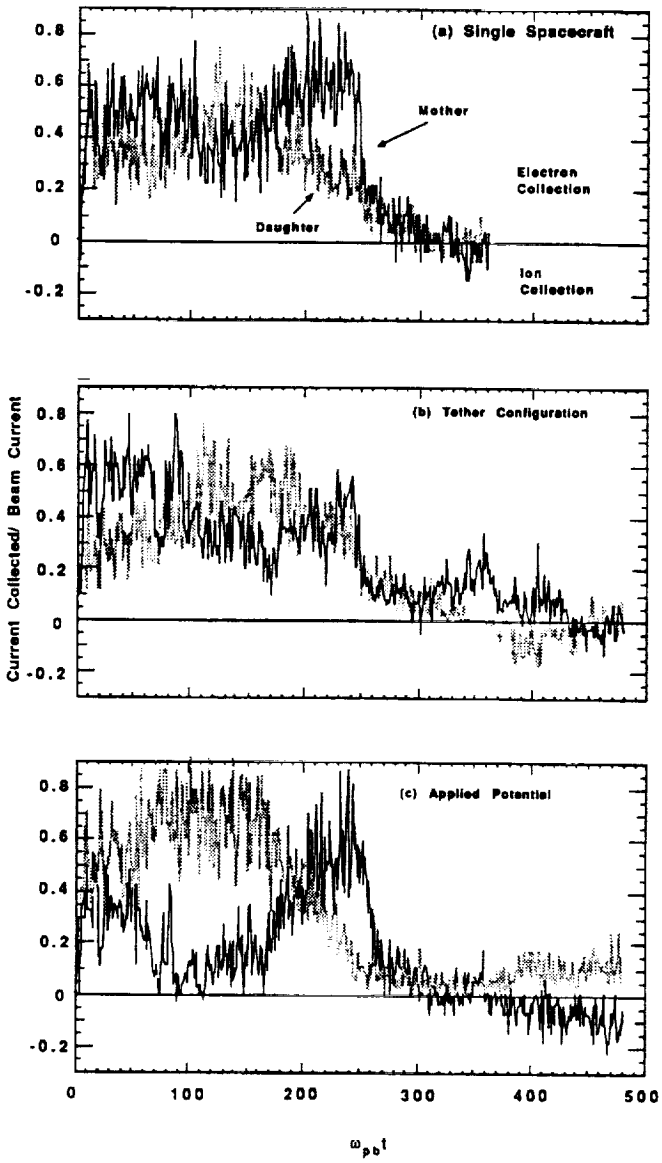

Fig. 4. Time histories of the spacecraft potential for the cases shown in Fig. 3.

recently investigated via particle simulations for the single spacecraft configuration [21]. In this section, the simulations are extended to the tether configuration. The same voltage as in Fig. 4b is applied between mother and daughter.

For these ionization processes to be important, the collision period must be comparable to or smaller than the time for the stagnation region to form. For the present parameters, the stagnation region forms in $\omega_{pb}t \lesssim 200$ so that for ionization processes to be important the collisional frequency ν_c must be greater than about $0.005\omega_{pb}$. In the following, ν_c is set at $0.01\omega_{pb}$. The corresponding evolution of the beam phase is shown in Fig. 5 when the

neutral are injected around the mother (left hand side) and the daughter (right hand side).

It is seen that in both cases a well defined stagnation region does not form. Instead, when the neutrals are around the mother payload, there is direct ionization by beam particles which rapidly builds a high density plasma of moderate energy in the beam region (as seen by the high phase space density in the region $100 \lesssim x/\Delta \lesssim 200$ and $-0.5 \lesssim v_x/v_{xb} \lesssim 0.5$). This latter plasma can be drawn into the spacecraft to provide return current if the mother payload becomes positively charged to overcome the slight net forward momentum of the ionized electrons.

While placing neutrals in the beam region is efficient in reducing the level of spacecraft charging, it has the disadvantage that it also leads to the development of strong turbulence in the beam region that cause the beam to loose its coherence. This turbulence is seen in Fig. 5a–c as the development of short scale length vortices. It has relatively short scaled length because the newly ionized plasma increases the local plasma frequency so that resonant interactions between beam and plasma particles is forced to move to higher k values.

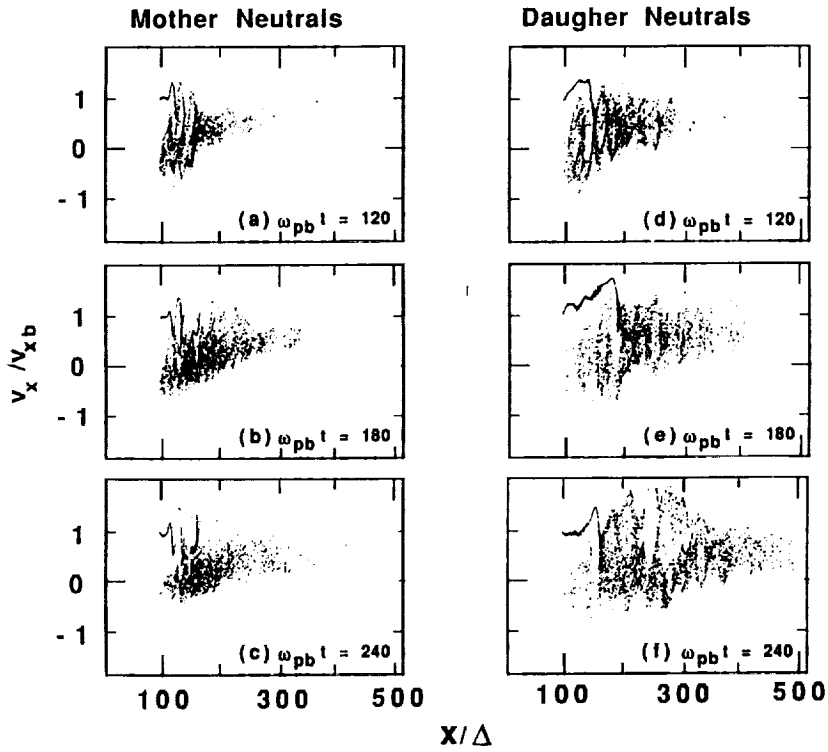

Fig. 5. The evolution of the beam phase space for the tether configuration with neutrals injected around the mother (left hand side) and from the daughter (right hand side).

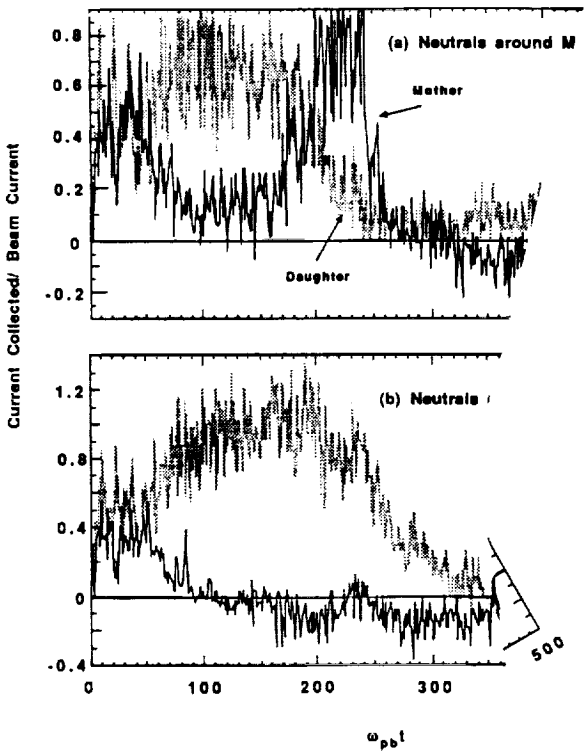

Fig. 6. The time histories of the payload potentials corresponding to the beam phase spaces in Fig. 5.

If instead, the neutrals are placed around the daughter payload then ionization can occur via vehicle induced ionization, i.e. if the daughter has a sufficiently high positive potential that the return current electrons attain ionization energies. This can be achieved by applying a voltage across the tether to make the daughter positively charged (in the present case to a few hundred volts). This method has the advantage that not only is the spacecraft charging reduced but it also minimizes beam distortion since the newly created plasma is well away from the beam region. This is seen in Figs. 5d and e where much of the beam is seen to propagate well away from the spacecraft with much less turbulence than seen in the counter parts for the mother-neutral case; at beam turn-off (Fig. 5f) a well defined beam is still seen out to $x/\Delta \simeq 300$ despite some induced turbulence.

The corresponding evolution of the spacecraft potential is shown in Fig. 6. As noted above, the case where the neutrals are injected around the mother, the mother has to charge to a sufficiently positive potential to draw the newly created plasma into the spacecraft. In the present case because the ionization threshold is set at three times the ambient thermal speed, the required potential is about a third of the beam energy, which is consistent with the simulation results. When more realistic ionization thresholds are utilized, the potential attained by the mother payload should be much

smaller. For the case when the neutrals are injected from the daughter, the return current can actually exceed the beam current (particularly when there is a high positive potential applied to the daughter), resulting in a decrease in the potential of both mother and daughter. As a result, the mother can be maintained at a low, even negative, potential during beam injection.

V. EFFECTS FROM THE MOTION OF THE SPACECRAFT

In the above simulations, the payloads were assumed stationary during the beam injection. This is not a restrictive assumption for sounding rocket experiments. However, because of the much higher speed of the space shuttle, ram and wake effects can develop which can possibly modify the beam-plasma interaction as well as the charging of the spacecraft. These effects are now examined through a comparison between the results from a stationary tether configuration (with no applied voltage) and when the mother and daughter payloads are moving across the field lines at a speed equal to twice the sound speed. In both cases, the mother and daughter are assumed to be initially separated by 32Δ.

One advantage of the motion of the spacecraft is that additional plasma can be swept into the spacecraft and help reduce the level of spacecraft charging. However, this is a relatively weak effect even when the spacecraft are travelling at twice the sound speed as illustrated in Fig. 7a. At early times when effects from the local depletion of the ambient plasma are small, the spacecraft potentials are approximately equal. However, after about $\omega_{pb}t \simeq 100$, the potential for the stationary spacecraft starts to increase at a faster rate than the potential for the moving spacecraft, reaching the beam energy at about $\omega_{pb}t \simeq 200$. The potential for the moving spacecraft remains below the beam energy throughout the period of injection and is about 20% below that of the stationary spacecraft at turnoff.

With the reduction in the spacecraft charging, the beam is able to generate slightly enhanced electromagnetic radiation as seen in Fig. 7b. Again this is only about a 20% increase for spacecraft moving at mach 2. The beam is also better able to propagate into the plasma, although it is again only a small change. This difference in beam propagation is illustrated in Fig. 8 which shows a full perspective of the beam phase space at $\omega_{pb}t = 180$ for injection from stationary spacecraft (left hand side) and from supersonic spacecraft. The bottom panels show the density of particles in the x–y plane, while the left and right panels show the v_x–x and v_x–y phases spaces, respectively. For the case of stationary spacecraft, there is strong reflection of beam particles at $x/\Delta \simeq 200$ (as indicated by the dashed line in the v_x–x panel) whereas this reflection occurs at about $x/\Delta \simeq 250$ for the case of supersonic spacecraft. In addition by $\omega_{pb}t = 240$

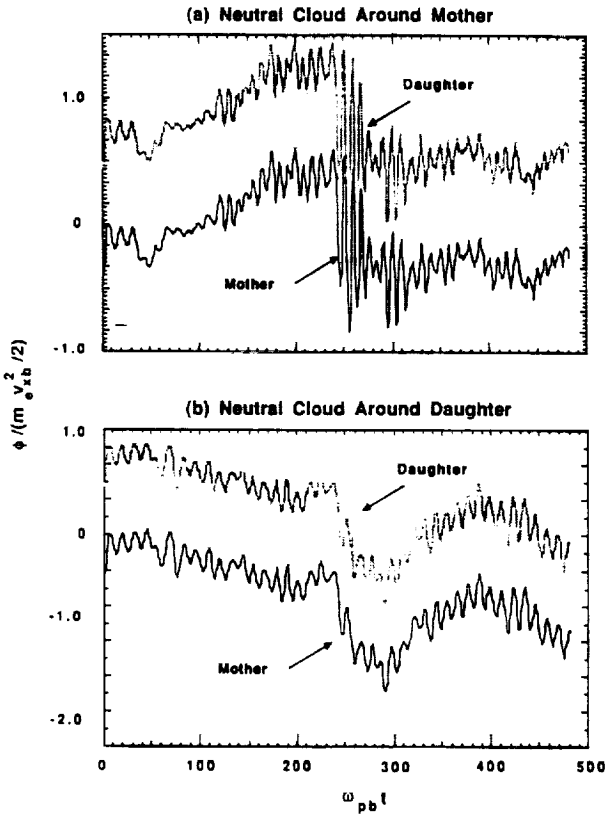

Fig. 7. Time histories of (a) the spacecraft potential and (b) the induced magnetic field for stationary spacecraft (dotted lines) and when the spacecraft are moving across the fields lines at twice the sound speed (solid lines).

(not shown), a well defined stagnation regions forms in the earlier case while in the latter case it is only just beginning to form.

Despite this enhanced penetration, beam distortion is enhanced via the increased turbulence induced by the motion of the spacecraft. For example, in both cases a sinusiodal trace is seen in the x–y panel near the spacecraft as the beam gyrates about the magnetic field. For the case of the stationary spacecraft, about one and a half gyrations can be identified in the density phase space before being smeared by turbulence while only about three quarters of a gyration can be seen on the right hand side. This enhanced turbulence is also seen in the v_x–x panels where there is stronger filling in of the phase space (particularly in the region $100 \lesssim x/\Delta \lesssim 200$) for the moving spacecraft. This difference arises because, for stationary spacecraft, the newly injected beam particles interact with essentially the same plasma so that at late times there is some saturation of the beam-plasma interaction. For injection from supersonic spacecraft, the newly injected

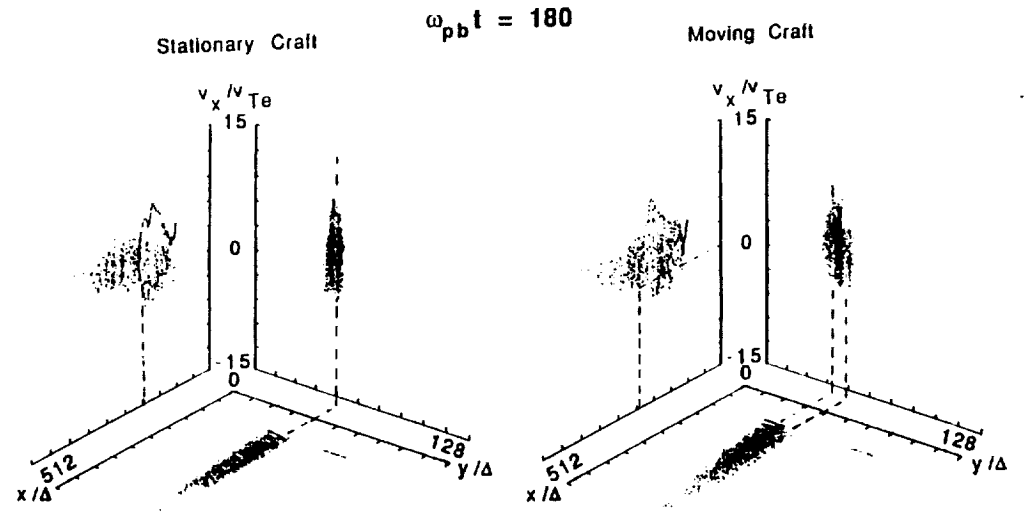

Fig. 8. Plots of the beam parallel velocity phases for injection from stationary spacecraft (left hand side) and from moving spacecraft (right hand side). The plot panels show density in coordinate space while the right and left hand panels show the v_x–x and v_x–y phase spaces, respectively.

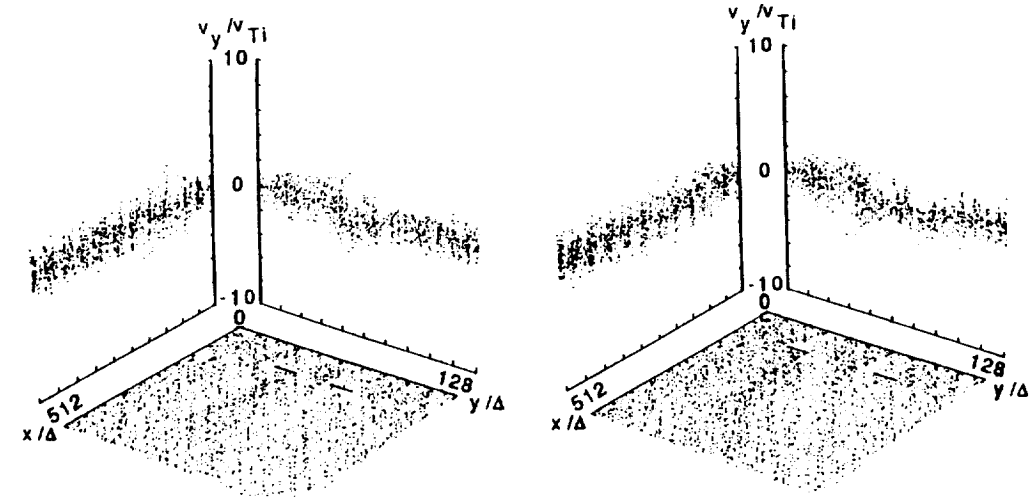

Fig. 9. As in Fig. 8, except for the ambient ion perpendicular velocity v_y.

beam particles interact with slightly different plasma, thereby allowing continual growth of the turbulence, albeit in slightly different regions.

Due to the presence of the enhanced turbulence, the highest energy beam particles are seen in the ram side of the beam as seen from the v_x–y panels. In the wake side, the energy of the beam particles is rapidly dissipated and the average speed of the particles is about 50% of that in the ram. Some of the beam particles which have been back-scattered and are in the wake miss the spacecraft before it moves across the field lines so that some of the beam particles propagate behind the spacecraft.

Probably the strongest effect associated with the motion of the spacecraft is in the heating and acceleration of the ambient ions, as illustrated in Fig. 9 which shows the ion perpendicular velocity v_y in the same format as Fig. 8. In both cases, as the beam is injected, the plasma ions are swept into the beam region to provide charge neutralization of the beam particles which have higher density than the ambient plasma [cf. *Winglee and Pritchett*, 1988]. This is seen as an enhancement in the ion density in the beam region in the x–y panels and, in the v_y–y panels as a positive acceleration in v_y for ions below the beam region (i.e. $y/\Delta \lesssim 32$) and a negative acceleration for ions above the beam region. These latter ions in the case of supersonic spacecraft are moving in the same direction as the spacecraft. As a result, those ions which have velocities comparable to the spacecraft experience an additional pull or acceleration as the beam regions moves across the field lines with the spacecraft. In the present example, these latter ions attain a maximum speed nearly twice that seen when the spacecraft are stationary.

VI. SUMMARY

In this paper, two-dimensional (three velocity) particle simulations have been used to investigate the injection and propagation of electron beams from spacecraft for a variety of different experimental configurations relevant to several recent and ongoing active beam experiments. These different configurations include injection from (i) a single spacecraft, (ii) a pair of electrically connected or tethered spacecraft, (iii) spacecraft immersed in high density neutral clouds and (iv) moving spacecraft.

It has been shown that in the absence of high density neutrals around the spacecraft, the local depletion of the ambient plasma via return currents into the spacecraft leads to the eventual strong charging of the spacecraft inhibiting the free propagation of the beam. Enhanced return currents can be attained through a tethered configuration, particularly if the passive (daughter) payload is biased positively, but plasma depletion and strong spacecraft charging still occur, albeit at later times. Increasing the speed of the spacecraft so that it moves through the plasma supersonically can further aid return-current collection but there is enhanced turbulence associated with the cross-field motion of the injection point so that strong beam distortion still occurs. There is also additional acceleration of ions in the ram of the beam.

An alternate way to reduce the spacecraft charging is via the injection of neutrals which are subsequently ionized by energetic electrons. However, the actual characteristics of the beam-plasma interaction depends on the region in which the neutrals are injected. If they are injected into the beam region, then ionization is predominately produced directly by the beam electrons. The amount of spacecraft charging is then limited to

a relatively small positive value that is required to stop the net forward momentum of the secondary electrons. The main disadvantage with this method is that enhanced short wavelength turbulence is induced via interactions of the newly created plasma and newly injected beam particles and this turbulence can destroy the coherence of the beam.

Alternately, the neutrals can be injected from the daughter. In this case, additional plasma can be produced by vehicle-induced ionization. This ionization is further enhanced if the daughter is biased positively so that energy of the return current electrons exceeds ionization threshold. This method was shown to be able to provide sufficient return current to maintain the beam-emitting payload at low (even negative) potential with the beam being able to easily propagate into the plasma with minimal distortion.

ACKNOWLEDGEMENTS

This research was supported by NASA grants NAGW-2471 and NAGW-1936 and NSF grant ATM 91-96132 to Southwest Research Institute.

REFERENCES

[1] R. A. Arnoldy, and J. R. Winckler, J. Geophys. Res., **86,** 575 (1981).
[2] J.R. Winckler, J. Spacecr. Rockets, **20**, 293, (1983).
[3] J. R. Winckler, J. E. Steffen, P. R. Malcolm, K. N. Erickson, Y. Abe and R. L. Swanson, J. Geophys. Res., **89**, 7565, (1984).
[4] J. R. Winckler, Y. Abe and K. N. Erickson, *Ion Acceleration in the Magnetosphere and Ionosphere*, Geophysical Monograph 38, AGU, 191, (1986).
[5] J. R. Winckler, et al., EOS, **70**, 657, 1989.
[6] R. L. Swanson, J. E. Steffen and J. R. Winckler, Planet. Space Sci., **34**, 411, (1986).
[7] D. A. Gurnett, W. S. Kurth, J. T. Steinberg, P. M. Banks, R. I. Bush and W. J. Raitt, Geophys. Res. Lett., **13,** 225, (1986).
[8] S. D. Shawhan, G. B. Murphy, P. M. Banks, P. R. Williamson and W. J. Raitt, Radio Sci., **19**, 471, (1984).
[9] Taylor, W.W.L., T. Obayashi, N. Kawashima, S. Sasaki, M. Yanagisawa, J.L. Burch, D.L. Reasoner and W.T. Roberts, Radio Sci., **20**, 486, (1985).
[10] T. Obayashi, and 12 others, Earth Orient. Applic. Space Technol., **5,** 37, (1985).
[11] S. Sasaki, N. Kawashima, K. Kuriki, M. Yanagisawa, and T. Obayashi, J. Spacecr. Rockets, **23**, 129, 1986.
[12] P. M. Banks, and W. J. Raitt, J. Geophys. Res., **93**, 5811 (1988).

[13] P. M. Banks, W. J. Raitt, A. B. White, R. I. Bush, and P. R. Williamson, J. Spacecr. Rockets, **24**, 138, (1987).

[14] B. N. Maehlum, J. Troim, N. C. Maynard, W. F. Denig, M. Friedrich, and K. M. Torkar, Geophys. Res. Lett., **15**, 725 (1988).

[15] W. F. Denig, N. C. Maynard, W. J. Burke and B. N. Maehlum, J. Geophys. Res., **96**, 3601 (1991).

[16] W. J. Raitt, P. R. Williamson, P. M. Banks, N. B. Myers and N. Kawashima, *Proc. of the 14th International Symposium on Space Tech. and Science*, 1501, (1984).

[17] Sasaki, S., K-I. Oyama, N. Kawashima, W. J. Raitt and N. B. Myers, EOS, **67**, 1170, (1986).

[18] B. E. Gilchrist, P. M. banks, T. Neubert, P. R. Williamson, N. N. Myers, W. J. Raitt, and S. Sasaki, J. Geophys. Res., **95**, 2469 (1990).

[19] T. Neubert and P. M. Banks, "Recent results from studies of electron beam phenomena in space plasmas", Planet. Space Sci., submitted (1991).

[20] R. M. Winglee, and P. J. Kellogg, J. Geophys. Res., **95**, 6167, (1990).

[21] R. M. Winglee, J. Geophys. Res., **95**, 6191, (1990).

[22] R. M. Winglee, and P.L. Pritchett, J. Geophys. Res., **93**, 5823, (1988).

APPENDIX B

SIMULATIONS OF RADIAL EXPANSION OF AN INJECTED ELECTRON BEAM

J. Koga and C. S. Lin[†]
Southwest Research Institute, San Antonio, TX 78228

ABSTRACT

To understand the radial expansion mechanism of an electron beam injected from a highly charged spacecraft, two-dimensional particle-in-cell simulations are conducted for a high density electron beam injected parallel to magnetic fields from an isolated equipotential conductor into a cold background plasma. The simulations indicate that charge buildup at the beam stagnation point causes the beam to exapnd radially to the beam electron gyroradius.

I. INTRODUCTION

In this paper we use computer simulations to examine the mechanism by which an electron beam radially expands after injection along magnetic field lines. The subject is of interest because the radial expansion affects the beam diameter and beam density, two critical parameters in determining the beam propagation and the instability conditions of a finite-radius electron beam [1].

Several two-dimensional simulations show that high density electron beams can propagate in a plasma because the net beam charge has caused the beam to expand radially and reduced the beam density [2–5]. For cross-field injection the beam is found to form a hollow cylinder of radius approximately equal to the beam electron gyroradius ρ_b, defined as the beam velocity v_b devided by the electron gyrofreuency Ω_{ce} [3]. In the case of parallel injection, the beam expands to fill a cyclinder with a radius smaller than ρ_b. However the radial expansion mechanism remains unclear for parallel beam injetions. This paper reports our simulation results about the radial expansion mechanism of an electron beam injected parallel to magnetic fields. In contrast to [4], we concentrate on the cases of high spacecraft charging.

[†] Present address: EOSP Applications, Inc., San Antonio, TX 78228

II. SIMULATION RESULTS

Realistic modeling of beam injection from a spacecraft requires injecting an electron beam from a finite isolated conductor. Using the capacity matrix method [4,6], we treat the spacecraft surface as a finite isolated equipotential conductor in an ambient plasma.

The simulation system contains 512×128 cells in the x and y coordinates. We use a periodic boundary condition for the lower and upper boundaries, and assume that the electric field at the left boundary and the potential at the right boundary are zero. The spacecraft is represented by a rectangular box centered at $x = 102\Delta$ and $y = 64\Delta$ with a size of $4\Delta \times 32\Delta$ in the x and y directions, respectively. The grid size, Δ, equals the Debye length of the ambient electrons defined as $\lambda_d = a_c/\omega_{pe}$ where $a_c = (2T_e/m_e)^{1/2}$ is the thermal velocity of the ambient electrons, ω_{pe} is the ambient electron plasma frequency, and T_e is the ambient electron temperature. The rato of ion to electron mass is 100, and $a_c = 0.001c$ where c is the speed of light, a unit of the simulation. The electron gyrofrequency Ω_{ce} is chosen to be $0.25\omega_{pe}$, close to the ionospheric value of $0.3\omega_{pe}$. The simulations have a time step $\Delta t = 0.05\omega_{pe}^{-1}$ and 131,072 particles for the ambient plasma. We have chosen the simulation parameters such that the beam has a density n_b much greater than the background density n_c ($n_b \gg n_c$) and a beam velocity much larger than the background thermal velocity ($v_b \gg a_c$). In the simulations, the electron beam has a width of 4Δ, an injection velocity of $v_b = 10a_c$ along the x axis, zero initial thermal velocity, and a density ratio of $n_b/n_c = 10$.

Figs. 1–3 show the simulaiton results at $\omega_{pe}t = 30$ when the simulations end. Fig. 1a plots beam electrons in the $v_x - x$ phase space, indicating that a large number of beam electrons are held close to the conductor surface. From a more detailed examination of the particle velocities near the conductor surface, we deduce that the stagnation point, where the injected electron velocity is significantly reduced, lies at about 2Δ away from the conductor surface.

Due to the high beam density the spacecraft becomes positively charged, causing the beam electrons to be rapidly drawn back to the spacecraft surface. The average electrostatic potential of the spacecraft in this case is $\approx 95\%$ of the beam energy. Some electrons at the front of the beam are accelerated to velocities higher than the original beam velocity, due to the bunching of beam electrons behind the beam head. Also some beam electrons returning to the conductor overshoot the conductor to the wake side. The configuration space plot (Fig. 1b) shows that the electron beam

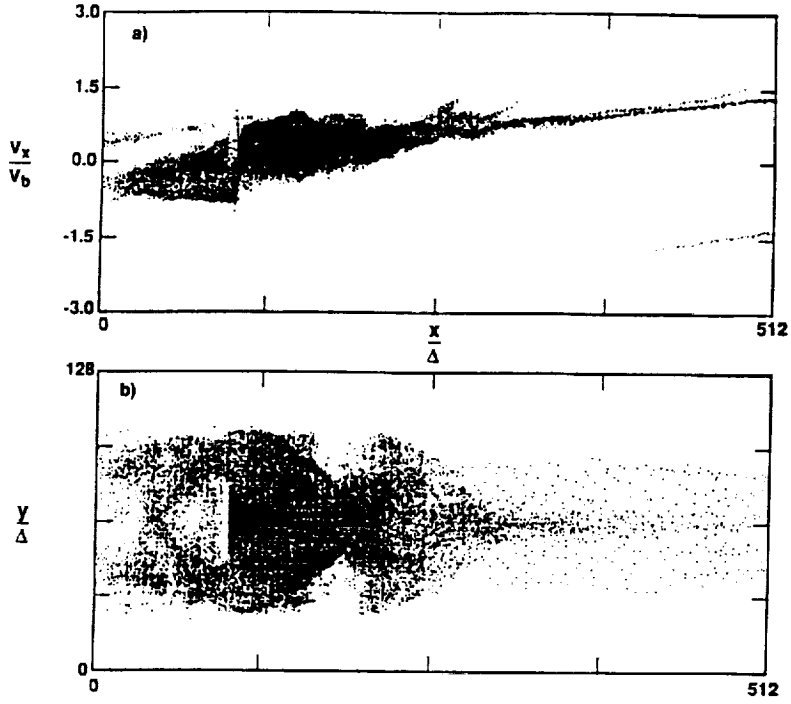

Figure 1. Simulation results for $n_b/n_c = 10$ and $v_b/a_c = 10$ at $\omega_{pe}t = 30$: (a) the phase space plot of the beam electrons in the $v_x - x$ coordinates and (b) the configuration plot of the beam electrons showing the electron positions in the $x - y$ plane.

expands radially. It appears that the maximum beam expansion occurs immediately after the stagnation point.

A contour plot of the beam density is presented in Fig. 2, where the outer contour line specifies the boundary of zero beam density and the inner coutour line specifies 10 beam electrons per cell (shaded area). The shaded area for high beam density is a small region very close to the conductor, which is represented in the figure as a vertical slit. Based on the contour plot, we deduce that the beam radius r_b is about 40Δ, approximately equal to the beam electron gyroradius ρ_b.

The bottom panel of Fig. 2, which plots the beam density averaged over the y coordinate versus x, further illustrates the concentration of beam electrons around the conductor surface. The beam density is highest at the stagnation point, in agreeement with analytical results for one-dimensional electron beam injection into a vacuum [7]. Physically, the beam density profile can be qualitatively explained by the conservation of flux $n_b v_b$. Because the average beam velocity is smallest at the stagnation point, the beam density should reach its maximum value there. However, beyond the

stagnation point, the beam density decreases as the beam expands transversely and the average beam velocity increases.

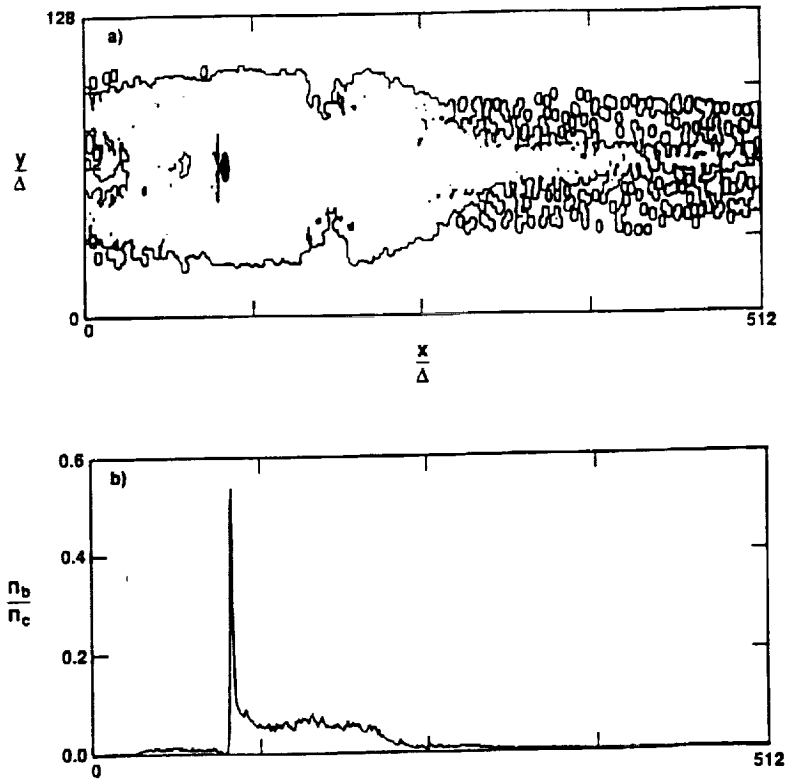

Figure 2. (a) Density contours of the beam electrons at $\omega_{pe}t = 30$. The outer contour line delineates the beam envelope and the small shaded area has more than 10 beam electrons per cell. The vertical slit near the shaded contour line represents the conductor. (b) profile of the beam density averaged over y.

To further understand the mechanism of radial expansion, we examine the transverse electric field E_y and the longitudinal electric field E_x. At each x coordinate, we find the maximum values of E_y and E_x along the y coordinate and plot them as a function of x (Figs. 3a and 3b). Comparing Figs. 3a and 3b with Fig. 2b, we note that the maximum transverse electric field E_y and the maximum longitudinal electric field E_x occur at the stagnation point, where the beam density is highest. The electric field profiles thus imply that the beam electrons gain their transvserse velocities mainly in the stagnation region. In general beam electrons travel through the stagnation region with velocities much lower than the initial beam velocity. So they spend more time in the stagnation region and are accelerated to higher velocities. After the stagnation region the transverse electric field E_y is smaller (Fig. 3a) and the average beam velocity is higher (Fig. 1a).

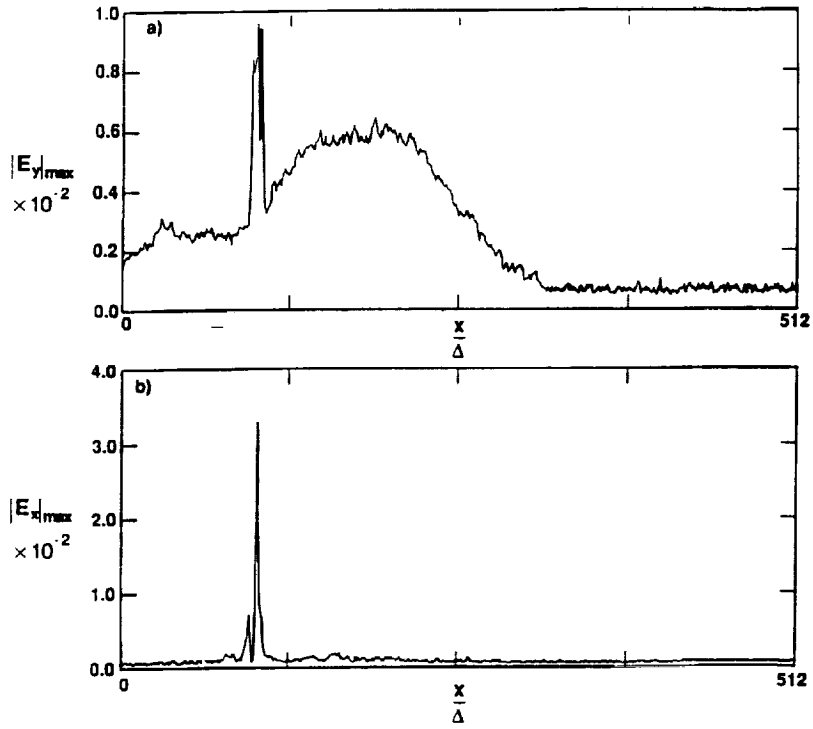

Figure 3. Profiles of the maximum transverse electric field (top) and the maximum longitudinal electric field (bottom). The maximum values are determined from a column of cells at each given x position.

Therefore, the beam electrons receive their largest tranverse kick very close to the spacecraft and experience smaller transverse acceleration from that point on.

The transverse velocities to which the beam electrons are accelerated depend on E_y and the duration the beam electrons spend in the stagnation region. The width of the large transverse electric field region is approximately 8Δ (Fig. 3a). From the maximum value of E_y and the average beam velocity in the large electric field region, we estimate that the beam electrons can gain a transverse velocity about $0.75v_b$. In the simulations the beam electron velocity v_y immediately after the stagnation point has a maximum value about v_b. As a result, the radius of the beam envelop is of the order of the beam electron gyroradius.

III. SUMMARY

We have examined the radial expansion mechanism of a high density electron beam injected parallel to magnetic fields into a background plasma. The simulations indicate that in high beam current cases ($n_b \gg n_c$

and $v_b \gg a_c$), the beam radius expands to the beam electron gyroradius. Previous simulations have indicated that the radius of a parallelly injected electron beam expands to about half the beam electron gyroradius for $n_b = 4n_c$ [4]. We have conducted a parameter survey to determine the dependence of the beam radius on beam denisty and other plasma paramters. Due to page limitation, the results will be reported separately.

The radial expansion is found to occur near the stagnation point, very close to the conductor surface for our parameters. It appears that the initial expansion determines the beam envelope after the stagnation point. The radial expandion is shown to be caused by charge buildup at the stagnation point, producing locally a large transverse electric field. Accelerated by the transverse electric field, the beam electrons injected parallel to magnetic fields receive a large transverse kick. The maximum perpendicular velocity gained by the beam electrons approaches the beam injection velocity.

In this paper we have concentrated on high beam current simulations relevant to significant spacecraft charging. Note that the conductor potential in our simulations reaches about 95% of the beam energy. The simulation results are thus most applicable to the SEPAC electron beam injection experiments on the Shuttle when it was charged to the beam energy.

ACKNOWLEDGEMENTS

We would like to thank R. M. Winglee for helpful suggestions on simulation techniques. The work was supported by NASA contract NAGW–1936 and by Lewis Research Center through NASA Contract NAS8-32488. The particle simulations were performed on the CRAY-YMP at NASA Ames Research Center and the CRAY-YMP at Goddard Space Flight center.

REFERENCES

[1] H. K. Wong and C. S. Lin, Radio Sci., **25**, 277, (1990).

[2] R. M. Winglee and P. L. Pritchett, J. Geophys. Res., **92**, 6114 (1987).

[3] H. Okuda and J. Berchem, J. Geophys. Res., **93**, 175 (1988).

[4] R. M. Winglee, and P. L. Pritchett, J. Geophys. Res., **93**, 5823 (1988).

[5] C. S. Lin and J. K. Koga, IEEE Trans. Plasma Sci., **17**, 205 (1989).

[6] R. W. Hockney and J. W. Eastwood, *Computer Simulation Using Particles* (McGraw-Hill, New York, 1981).

[7] D. E. Parks, A. R. Wilson, and I. Katz, IEEE trans. Nucl. Sci., **NS-22**, 2368 (1975).